

Comparative study on brightness temperature reconstruction of synthetic aperture based on deep learning

Ziyu Sun^{1,a}, Hao Li^{1,b}

¹China Academy of Space Technology, Xi'an 710100, China

^a 18220369522@163.com, ^b lihao714925@163.com

Abstract: In order to study the effect of deep learning method in the brightness temperature reconstruction of synthetic aperture radiometer, the gray value of remote sensing image with channel amplitude-phase error and random error is used as the original brightness temperature image for simulation experiment to compare the brightness temperature reconstruction images under traditional Fourier transform, CNN inversion, U-net inversion and Resnet inversion. From the view of image visual effect, Resnet inversion method has the best image restoration effect and the weakest background noise. From the evaluation index, the RMSE of Resnet inversion method is the smallest, which is 6.28K, and the PNSR value is the highest, which is 31.62dB. The second is CNN inversion method, RMSE value is 10.93K, PNSR value is 27.09dB. Therefore, Resnet inversion method can better restore bright temperature image, reduce Gibbs effect and improve image resolution.

Keywords: Deep learning, Bright-temperature reconstruction, Synthetic aperture microwave radiometer

1. Introduction

Most of the existing studies focus on one-dimensional antenna or two-dimensional U-array antenna experiments[9], while Y-array antenna has a wide range of practical applications and the sampling principle of Y-array is different from that of U-array. Compared with rectangular sampling, Y-array has a higher sampling rate and more complex data processing. Therefore, this paper studies the Y-array antenna and compares the effect of brightness temperature reconstruction under different deep learning networks.

2. Related Theories and Methods

2.1 Principle of Synthetic Aperture Microwave Radiation Imaging

The synthetic aperture radiometer uses a small aperture antenna instead of a large aperture antenna to receive the scene radiation signal and obtain the spatial frequency distribution of the original scene brightness temperature, that is, the visibility function. The synthetic aperture radiometer is composed of several binary interferometers, as shown in Figure 1.

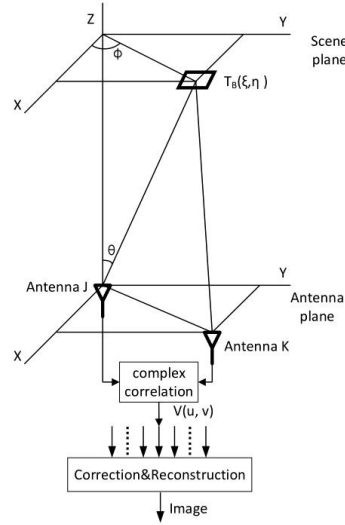


Fig.1 Schematic of the interference measurement

Let $f_i(\sigma)$ and $f_k(\sigma)$ represent the antenna transfer voltage function at P_i and P_k respectively, and $E(\sigma, P_i, t)$ and $E(\sigma, P_k, t)$ represent the electric field intensity generated by surface source σ at antenna P_i and P_k respectively, then the output voltage $U_i(t)$ and $U_k(t)$ of the two receiving antennas are:

$$U_i(t) = \sum_{d\sigma \in A} E(\sigma, P_i, t) f_i(\sigma) \quad (1)$$

$$U_k(t) = \sum_{d\sigma \in A} E(\sigma, P_k, t) f_k(\sigma) \quad (2)$$

The mutual power spectral density of the output voltage of the two antennas is:

$$\begin{aligned} S_{U_i, k}(f) &= \sum_{d\sigma \in A} F\{E(\sigma, P_i, t) E(\sigma, P_k, t + \tau)\} f_i(\sigma) f_k(\sigma) \\ &= \sum_{d\sigma \in A} \frac{e^{j2\pi f(R_i - R_k)/c}}{R_i R_k} S_E(\sigma, f) f_i(\sigma) f_k(\sigma) \end{aligned} \quad (3)$$

Assuming that the antenna far-field condition is satisfied between the spreading source A and the antenna P_i and P_k , the cross-power spectral density of the output voltage can be simplified as:

$$S_{U_i, k}(f) = \frac{Z}{2} \sum_{d\sigma \in A} B_f(\sigma, P_i, f) f_i(\sigma) f_k(\sigma) e^{j2\pi(D_x l + D_y m)/\lambda} d\Omega \quad (4)$$

Output of a complex correlation receiver:

$$V = 2 \int_0^\infty S_{U_i, k}^*(f) H_i(f) H_k^*(f) df \quad (5)$$

When the striping effect and constant coefficient are ignored, the visibility function can be simplified to:

$$V(u_{ik}, v_{ik}) = \iint_{l^2 + m^2 \leq 1} T'_{ik}(l, m) e^{-j2\pi(u_{ik}l + v_{ik}m)} dldm \quad (6)$$

Where, the modified brightness temperature $T'_{ik}(l, m) = \frac{D_0}{4\pi} \frac{T_B(l, m)}{\sqrt{1 - l^2 - m^2}} F_n(l, m)$, $F_n(l, m)$ represents the unit antenna normalized graph, and D_0 represents the maximum directivity of the unit antenna.

As can be seen from equation (6), the two-dimensional Fourier transform relationship between the visibility function and the modified brightness temperature is exactly satisfied.

2.2 Deep Learning Network

2.2.1 CNN

Convolutional neural network is a kind of deep neural network with convolutional structure, the structure of convolutional neural network includes: convolutional layer, pooling layer, fully connected layer. Each layer has multiple feature maps, each feature map extracts a feature of the input through a convolution filter, and each feature map has multiple neurons.

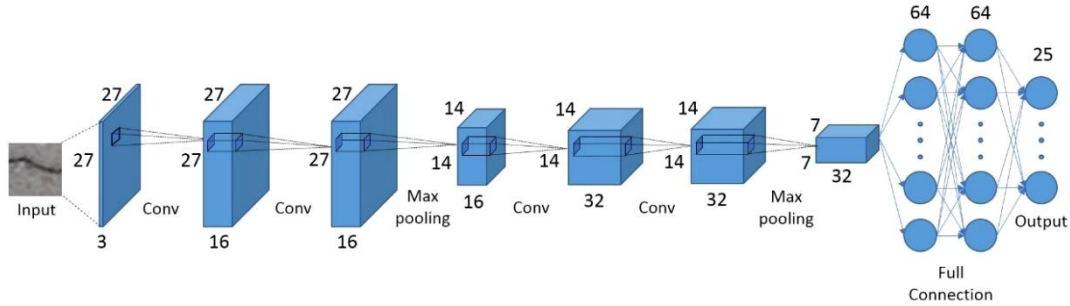


Fig.2 CNN network structure

2.2.2 U-net

The structure of UNet consists of two parts: Encoder and Decoder. The encoder consists of multiple convolution blocks, each consisting of a convolution layer (usually a 3x3 convolution kernel), Batch Normalization, and an activation function (usually a ReLU), followed by a pooling layer. The decoder consists of multiple deconvolution blocks, after which an upper sampling layer is added to increase the size of the feature map.

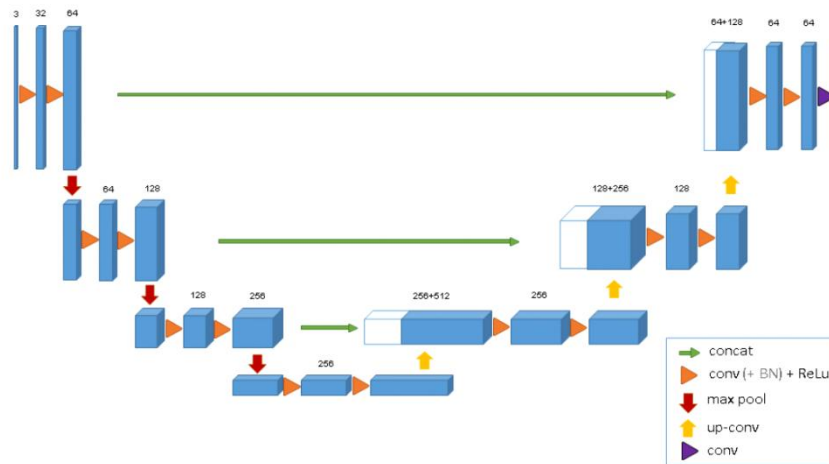


Fig.3 U-net network structure

2.2.3 Resnet

Resnet is proposed to solve the degradation problem of deep neural network (DNN) when there are too many hidden layers. Resnet can gradually extract information from low-resolution images and add back the missing details through the addition operation of residual images. This allows the network to perform image recovery or other tasks more efficiently, improving the model's performance and accuracy.

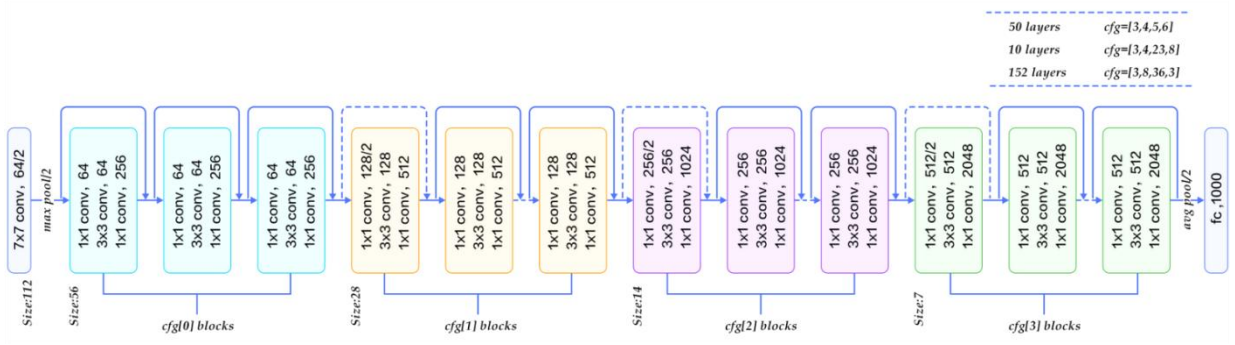


Fig.4 Resnet network structure

3. Result Analysis

3.1 Image Comparison

In this experiment, 9300 scene images were selected as the training set and 600 scene images were selected as the test set for network training. Fig.5 shows the brightness temperature distribution of the original scene, and Fig. 6 shows the brightness temperature reconstruction image under different inversion methods.

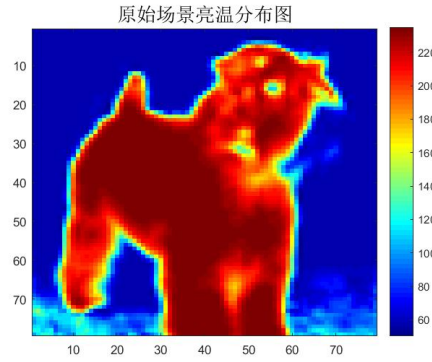
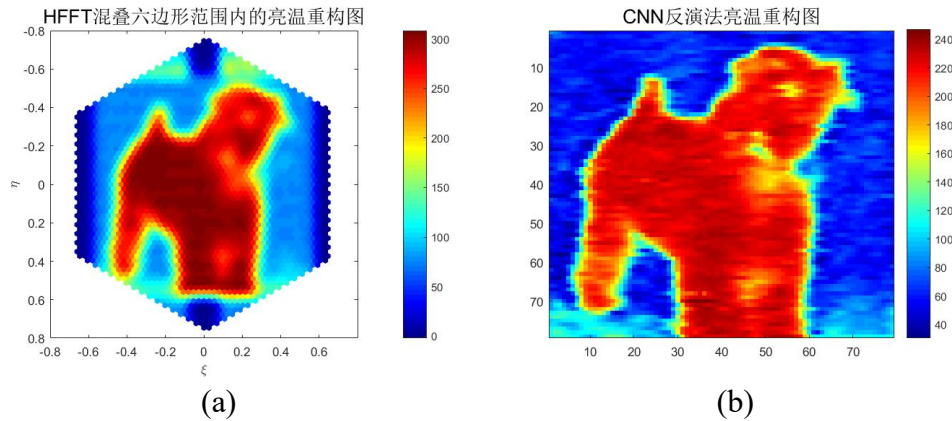


Fig.5 Original brightness temperature



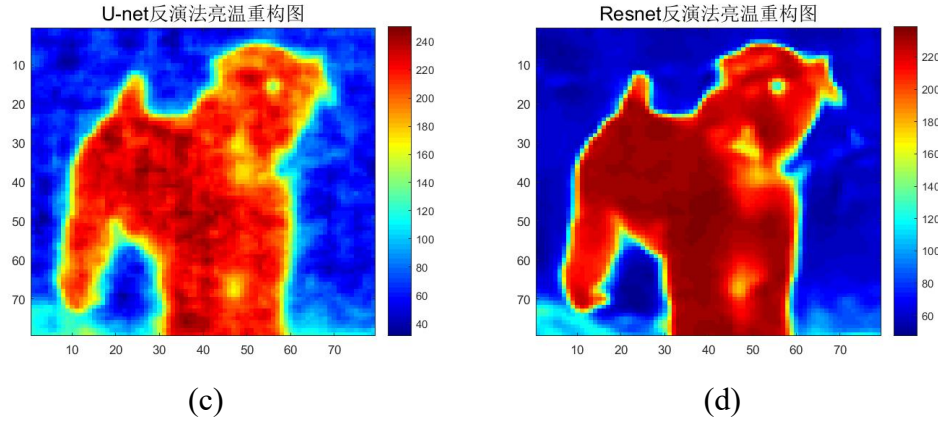


Fig.6 Brightness temperature composition under different methods

In Fig. 6, (a) shows the bright temperature and weight composition of HFFT inversion method within the range of alix-hexagon, (b) shows the bright temperature and weight composition of CNN inversion method, (c) shows the bright temperature and weight composition of U-net inversion method, and (d) shows the bright temperature and weight composition of Resnet inversion method. From the visual effect of the image, it can be seen that Resnet method has the best restoration effect on the original brightness and temperature, with the least noise, and can restore the original brightness temperature better, followed by cnn method. The noise of U-net reconstruction is too large, the Gibbs effect is obvious, and the restoration effect is poor. However, some details of the reconstructed image with Resnet method are not obvious, such as the mouth of the dog in the original scene.

3.2 Index Comparison

Table 1. Comparison of reconstruction results by different methods

Evaluation index	HFFT	CNN	U-net	Resnet
RMSE(K)	15.80	10.93	13.57	6.28
PNSR(dB)	23.88	27.09	24.89	31.61

Table 1 shows the evaluation indexes of reconstructed image results under different methods, which are evaluated from two aspects: mean square error and signal-to-noise ratio. RMSE value of HFFT inversion algorithm is 15.80K, PNSR value is 23.88dB, RMSE value of CNN inversion algorithm is 10.93K, PNSR value is 27.09dB, RMSE value of U-net inversion algorithm is 13.57K, PNSR value is 24.89dB. The RMSE value and PNSR value of Resnet inversion algorithm are 6.28K and 31.61dB.

4. Summary

In this paper, three deep learning network methods are designed for the bright temperature reconstruction of synthetic aperture microwave radiometer, namely, CNN, U-net and Resnet method. Compared with the traditional HFFT inversion method, the reconstruction effect of deep learning method can better restore the original bright temperature image. The Resnet method has the best restoration effect, and the mean square error can be reduced to one third of the HFFT method. Compared with the other three methods, the Gibbs effect is also significantly reduced, and the image signal-to-noise ratio and image resolution are improved.

Future and prospects: 1. This experiment is only a simulation experiment, and the measured data of the synthetic aperture microwave radiometer will be tested in the future. 2. There is some noise in the background of the reconstructed image with Resnet method, and the reconstruction effect can be further improved.

Acknowledgements

National Natural Science Foundation of China(42306203) 、 Young Star of Science and Technology in Shaanxi Province(2023KJXX-104)

References

- [1] 李一楠,周武,窦昊锋,等.高分辨星载海洋微波辐射测量技术发展综述[J].空间电子技术,2024,21(02):1-16+113.
- [2] A. Camps, J. Bará, I. C. Sanahuja, F. Torres. The processing of hexagonally sampled signals with standard rectangular techniques: Application to 2-D large aperture synthesis interferometric radiometers. IEEE Transactions on Geoscience and Remote Sensing, 1997, 35(1): 183-190.
- [3] Tanner,A. B., Calvin T. Swift. Calibration of a synthetic aperture radiometer. IEEE Trans. Geosci. Remote Sens. 1993, 31(1): 257-256.
- [4] Eric Anterrieu. A resolving matrix approach for synthetic aperture imaging radiometers. IEEE Trans. Geosci. Remote Sensing, 2004, 42(8): 1649-1656.
- [5] ZHANG Y, REN Y, MIAO W, et al. Microwave SAIR Imaging Approach Based on Deep Convolutional Neural Network[J/OL]. IEEE Transactions on Geoscience and Remote Sensing, 2019, 57(12): 10376-10389.
- [6] DOU H, XIAO C, LI H, et al. Deep Learning Imaging for 1-D Aperture Synthesis Radiometers[J/OL]. IEEE Transactions on Geoscience and Remote Sensing, 2023, 61: 1-16.
- [7] XIAO C, DOU H, LI H, et al. Image Reconstruction of Synthetic Aperture Radiometer by Transformer[J/OL]. IEEE Transactions on Geoscience and Remote Sensing, 2023, 61: 1-15.
- [8] 翟韧. 基于深度学习的综合孔径辐射计成像方法研究[D]. 华中科技大学,2022.DOI:10.27157/d.cnki.ghzku.2022.001759.
- [9] 刘子力,杨家俊,王文静,等.遥感图像云检测方法综述[J].中国空间科学技术,2023,43(01):1-17.DOI:10.16708/j.cnki.1000-758X.2023.0001.